Properties of a dielectric plate using entangled two-photon states*

Zhou Zhi-Yuan(周志远), Ding Dong-Sheng(丁冬生), Shi Bao-Sen(史保森)†,
Zou Xu-Bo(邹旭波), and Guo Guang-Can(郭光灿)

Key Laboratory of Quantum Information, University of Science and Technology of China, Hefei 230026, *China*

(Received 28 November 2011; revised manuscript received 28 February 2012)

We theoretically study the properties of a dielectric plate with a modified Hong–Ou–Mandel interferometer. The fourth-order correlation functions are calculated in two regimes divided depending on the relative size between the thickness of dielectric plate and one-photon coherence length. When the thickness of dielectric plate is less than the one-photon coherence length, a novel modulation behavior of the coincidence rate is observed, which has not been discussed before. If the thickness of dielectric plate is larger than the one-photon coherence length, the coalescence and anti-coalescence are observed. The results obtained highlight the effects of linear optical element on the fourth-order interference.

Keywords: entangled two-photon states, dielectric plate, coherence length

PACS: 42.50.Dv, 42.65.Lm **DOI:** 10.1088/1674-1056/21/9/094204

1. Introduction

The entangled photon pair generated in the process of spontaneous parametric down conversion (SPDC)[1] is highly correlated in time, and this property has been used for measurements with sub-femtosecond time resolution.[2] Moreover, the entangled photon pairs have also been used to obtain the absolute quantum efficiencies of detectors.[3] Properties of entangled photon pairs make it suitable for testing quantum mechanics against local hidden-variable theory in different physical situations.[4] Photon pairs entangled in polarization have also been applied in quantum cryptography[5] and quantum teleportation recently.[6] All these applications are essential in the field of quantum information.[7]

The time entanglement of photons in a pair can be revealed by coincidence count measured in Hong–Ou–Mandel (HOM) interferometer.[1,8] Generally, a dip occurs at the coincidence count rate with the width given by entanglement time (typically tens or hundreds of femtoseconds). Since the emergence of HOM interferometer, several modified schemes have been studied both theoretically and experimentally. The modified scheme is constructed by inserting an optical cavity[9,10] or a dispersive optical element[11] into arms of the original one. Furthermore, the entanglement properties have been broadly studied in other physical situations.[12−14] These studies further characterize the properties of entangled photons in a pair.

In this work, we investigate the quantum properties of a dielectric plate using entangled photons in a pair from SPDC. According to the quantum input–output relation of a dielectric calculated in Ref. [15], the fourth-order correlation function is calculated. Here we regard the dielectric plate as a four-port device. We show that the response of the dielectric plate varies with its thickness and quite different behaviors are observed in two regimes which are divided according to the relative size between the plate thickness and one-photon coherence length.[16] When the thickness of the plate is less than the one-photon coherence length, a novel modulation behavior is observed, and the modulation amplitude is sensitive to the refractive index of the dielectric plate. The calculated results show that the modulation only changes the intensity of coincidence count rate, but the visibility is independent of this modulation. However, when the thickness of the plate is larger than the one-photon co-

*Project supported by the National Natural Science Foundation of China (Grant Nos. 10874171 and 11174271), the National Fundamental Research Program of China (Grant No. 2011CB00200), the Innovation Fund from Chinese Academy of Sciences, and the Program for New Century Excellent Talents in University of China (Grant No. NCET-07-0791).

†Corresponding author. E-mail: drshi@ustc.edu.cn

© 2012 Chinese Physical Society and IOP Publishing Ltd

herence length, we observed recurrent dips and peaks due to destructive and constructive interference of different Feynman paths. Additionally, the influence of the bandwidth of interference filter is also investigated with the thickness of the plate unchanged.

A practical HOM interferometer usually contains linear optical elements such as a lens, a prism, a beam splitter, and a cavity. Some of them can be viewed as a dielectric plate. By means of the simple model we study here, the quantum properties of these linear optical elements can be characterized quantitatively. For simplicity, we only consider a bulk dielectric plate with no absorption and dispersion. However, the used method and obtained results in this work can be definitely generalized to much more complex cases, such as absorptive and dispersive materials, and a stack of plates with different refractive indexes.

2. Model

The model we used in our calculation is shown in Fig. 1. A continuous 425-nm pump field passes through a 3-mm-long BBO crystal, and a pump photon will be split into a signal photon and an idler photon centered at 850 nm with certain probability. We consider the degenerated type-I phase-matched down conversion, where two down-converted photons have the same polarization. After being directed by mirrors M1 to M6, the idle and signal photons recombine at a 50:50 beam splitter (BS). A transparent dielectric plate with thickness of l and refractive index of n is inserted in the signal arm of the HOM interferometer. The relative path difference of the two arms can be adjusted through the translation of M2 and M3 mounted on a translation stage. In front of each single-photon detector, there is an interference filter centered at 850 nm. The signals from detectors D1 and D2 are sent to a coincidence count device.

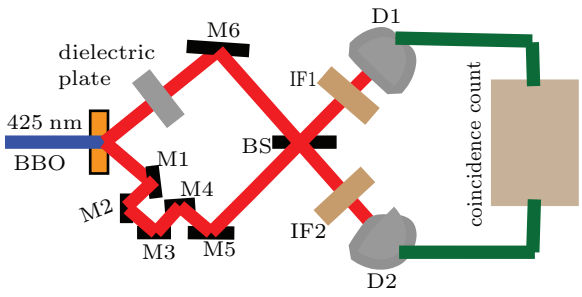


Fig. 1. (colour online) Schematic of HOM interferometer with a dielectric plate. M1–M6: mirror; BS: beam splitter; IF1, IF2: interference filter; D1, D2: single-photon detector.

3. Calculation of fourth-order correlation function

The two-photon state generated due to SPDC can be written as follows:[17]

$$|\Psi\rangle = \int_0^{\omega_\mathrm{p}} \mathrm{d}\omega\phi(\omega)\hat{a}_\mathrm{s}^+(\omega)\hat{a}_\mathrm{i}^+(\omega_\mathrm{p}-\omega)\,|\mathrm{vacuum}\rangle\,, \quad (1)$$

where ω_p is the pump light frequency, ω is the signal frequency, $\omega_\mathrm{p}-\omega$ is the conjugate idler frequency, $\varphi(\omega)$ is the function with a peak at $\omega=\omega_\mathrm{p}/2$ which is introduced by the phase-matching condition, and $\hat{a}_\mathrm{s}^+(\omega)$ and $\hat{a}_\mathrm{i}^+(\omega_\mathrm{p}-\omega)$ are creation operators for signal and idler photons at the corresponding frequency, respectively.

The electric fields $\hat{E}_1$ and $\hat{E}_2$ at photodetectors D1 and D2 can be written as

$$\hat{E}_1^{(+)}(t) = \hat{F}_\mathrm{A}\Big[\sqrt{T}\hat{E'}_\mathrm{s}^{(+)}(t-\tau_1) + \mathrm{i}\sqrt{R}\hat{E}_\mathrm{i}^{(+)}(t-\tau_1+\delta\tau)\Big], \quad (2)$$

$$\hat{E}_2^{(+)}(t) = \hat{F}_\mathrm{B}\Big[\sqrt{T}\hat{E}_\mathrm{i}^{(+)}(t-\tau_1) + \mathrm{i}\sqrt{R}\hat{E'}_\mathrm{s}^{(+)}(t-\tau_1-\delta\tau)\Big], \quad (3)$$

where $R=1/2$ and $T=1/2$ are the reflectivity and transmissivity of the BS, τ_1 is the propagation time, $\delta\tau$ is the relative delay of the two arms, $\hat{F}_\mathrm{A}$ and $\hat{F}_\mathrm{B}$ are operators of the interference filters IF1 and IF2, and $\hat{E'}_\mathrm{s}=G\hat{E}_\mathrm{s}$ with $\hat{G}$ being the transfer function of the dielectric plate inserted in the beam. In Ref. [15], the input and output of a dielectric slab is deduced. If the characteristic absorption of the material can be ignored, the function G can be expressed as follows:

$$G(\omega) = \frac{4n\exp[\mathrm{i}(n-1)\omega l/c]}{(1+n)^2-(1-n)^2\exp(2\mathrm{i}n\omega l/c)}, \quad (4)$$

and

$$|G(\omega)|^2 = \frac{4n^2}{4n^2+(1-n^2)^2\sin^2(n\omega l/c)}. \quad (5)$$

We denote the frequency response of the interference filters IF1 and IF2 by $f_1(\omega)$ and $f_2(\omega)$, respectively, and $f_1(\omega)=f_2(\omega)=f(\omega)=\exp[-(\omega-\omega_\mathrm{p}/2)^2/4\Delta\omega^2]$ with $\Delta\omega$ being the bandwidth of the IF. We perform Fourier transforms of Eqs. (2) and (3), and then obtain

$$\hat{E}_\mathrm{s}^{(+)}(t) = \int_0^{+\infty}\mathrm{d}\omega\hat{a}_\mathrm{s}(\omega)\,\mathrm{e}^{-\mathrm{i}\omega t}, \quad (6)$$

$$\hat{E}_{\rm i}^{(+)}(t) = \int_0^{+\infty} {\rm d}\omega \hat{a}_{\rm i}(\omega)\,{\rm e}^{-{\rm i}\omega t}, \quad (7)$$

$$\hat{E}'^{(+)}_{\rm s}(t) = \int_0^{+\infty} {\rm d}\omega G(\omega)\hat{a}_{\rm s}(\omega)\,{\rm e}^{-{\rm i}\omega t}, \quad (8)$$

$$\hat{E}_1^{(+)}(t) = \int_0^{+\infty} {\rm d}\omega \frac{1}{\sqrt{2}}\big(G(\omega)\hat{a}_{\rm s}(\omega)\,{\rm e}^{-{\rm i}\omega(t-\tau_1)} + {\rm i}\hat{a}_{\rm i}(\omega)\,{\rm e}^{-{\rm i}\omega(t-\tau_1+\delta\tau)}\big) f(\omega), \quad (9)$$

$$\hat{E}_2^{(+)}(t) = \int_0^{+\infty} {\rm d}\omega \frac{1}{\sqrt{2}}\big(\hat{a}_{\rm i}(\omega)\,{\rm e}^{-{\rm i}\omega(t-\tau_1)} + {\rm i}G(\omega)\hat{a}_{\rm s}(\omega)\,{\rm e}^{-{\rm i}\omega(t-\tau_1-\delta\tau)}\big) f(\omega). \quad (10)$$

The joint probability P_{12} of detecting two photons by detector D1 and D2 at time t and $t+\tau$ is given by[18]

$$P_{12}(\tau) = K\langle\Psi|\,\hat{E}_1^{(-)}(t)\hat{E}_2^{(-)}(t+\tau)\hat{E}_2^{(+)} \times (t+\tau)\hat{E}_1^{(+)}(t)\,|\Psi\rangle\,, \quad (11)$$

where K is a constant. Combining Eqs. (1), (9), (10), and (11), we obtain

$$P_{12}(\tau) = \frac{K}{4}\Big[\,\Big|g_{12}^{(1)}(-\tau)\Big|^2 + \Big|g_{12}^{(2)}(2\delta\tau-\tau)\Big| - \Big(g_{12}^{(1)}(-\tau)g_{12}^{*(2)}(2\delta\tau-\tau)+{\rm c.c.}\Big)\Big]. \quad (12)$$

The definitions of $g_{12}^{(1)}(\tau)$ and $g_{12}^{(2)}(\tau)$ is given in Appendix A. In practice, the resolving time of the detector is much longer than the time range of functions $g_{12}^{(1)}(\tau)$ and $g_{12}^{(2)}(\tau)$, and therefore we can integrate the terms in Eq. (12) from $-\infty$ to $+\infty$. Then we obtain the coincidence rate

$$\begin{aligned} &R_{\rm C}(\delta\tau)\\ &= \int_{-\infty}^{+\infty} {\rm d}\tau P_{12}(\tau)\\ &= \frac{K}{4}\int_{-\infty}^{+\infty} {\rm d}\omega[(|\phi(\omega+\omega_0)|^2 f^4(\omega)\,|G(\omega+\omega_0)|^2\\ &+ |\phi(\omega_0-\omega)|^2 f^4(\omega)\,|G(\omega_0-\omega)|^2)\\ &- (\phi(\omega_0-\omega)\phi^*(\omega_0+\omega)f^4(\omega)\\ &\times G^*(\omega_0-\omega)G(\omega_0+\omega)\exp(2{\rm i}\omega\delta\tau)\\ &+ {\rm c.c.})]. \end{aligned} \quad (13)$$

Assuming that $\varphi(\omega_0+\omega)$ and $\varphi(\omega_0-\omega)$ change slowly within the bandwidth of $f(\omega)$, then we can neglect $\varphi(\omega)$ in the integration. Equation (13) is simplified to be

$$\begin{aligned} R_{\rm C}(\delta\tau) &= \frac{K}{4}\left[\int_{-\infty}^{+\infty} {\rm d}\omega f^4(\omega)\,|G(\omega+\omega_0)|^2 + \int_{-\infty}^{+\infty} {\rm d}\omega f^4(\omega)\,|G(\omega_0-\omega)|^2\right]\\ &- \int_{-\infty}^{+\infty} {\rm d}\omega f^4(\omega)G(\omega+\omega_0)\\ &\times G^*(\omega_0-\omega)\exp(2{\rm i}\omega\delta\tau) + {\rm c.c.}\\ &= \frac{K}{2}\int_{-\infty}^{+\infty} {\rm d}\omega f^4(\omega)\left[|G(\omega_0+\omega)|^2 - G(\omega+\omega_0)\,G^*(\omega_0-\omega)\exp(2{\rm i}\omega\delta\tau)\right]. \end{aligned} \quad (14)$$

Equation (14) is the expression we used to perform numerical calculation. In the sections below, we will study the coincidence count interference profiles as functions of different parameters.

4. Coincidence count rate versus plate thickness

Now we study coincidence count rate as a function of plate thickness, while keeping other parameters constant. It is obvious that when $l=0$ and $G(\omega)=1$, we obtain the well-known expression for the coincidences of HOM interferometer without the dielectric plate. That is

$$R(\delta\tau) = 1-\exp[-(\Delta\omega\delta\tau)^2], \quad (15)$$

where a constant multiplier is omitted since we are only interested in the coincidence count rate. First, the case (denoted by I) that the thickness l is much smaller than the one-photon coherence length $L = \lambda^2/\Delta\lambda$($\lambda$ and $\Delta\lambda$ are the central wavelength and bandwidth of the signal photon, respectively) is considered. If $\Delta\omega l/c \ll 1$ (or $l \ll \lambda^2/\Delta\lambda$) is satisfied for sufficiently small l, the function $|G(\omega+\omega_0)|^2$ varies slightly within the bandwidth of $f^4(\omega)$, and thus we can extract it out of the integration. Then equation (14) can be written by

$$\begin{aligned} R(\delta\tau) &\approx |G(\omega_0)|^2\left\{1-\exp[-(\Delta\omega\delta\tau)^2]\right\}\\ &= \frac{4n^2}{4n^2+(1-n^2)\sin^2(n\omega_0 l/c)}\\ &\times \left\{1-\exp[-(\Delta\omega\delta\tau)^2]\right\}. \end{aligned} \quad (16)$$

Equation (16) shows that the coincidence count rate is modulated by $|G(\omega_0)|^2$, and the modulation amplitude is a function of l and n. The modulation period is $\lambda/2n$. Figure 2 shows numerical calculations derived from Eq. (14), where bandwidth of the IF is $\Delta\lambda = 10$ nm ($\Delta\omega = 2\pi c\Delta\lambda/\lambda^2$), and refractive index of the plate is $n = 2.1$. We choose the value of l in order that the signal photon phase inside the plate is $\delta\phi = 2m\pi$, $2m\pi+\pi/2$, and $2m\pi+\pi$ (m is an integer). Figure 2(b) shows the three-dimensional (3D) plots of coincidence count rate as functions of l and $\delta\tau$, from

which we can see that there are two periods as l varies from $5\lambda/n$ (2.02381 μm) to $6\lambda/n$ (2.42857 μm). The ratio of the maximum and minimum of the coincidence count rate is consistent with the prediction given by Eq. (16). The maximum and minimum values are due to the resonance and anti-resonance of the signal photon inside the plate, respectively. As l is much smaller than the one-photon coherence length, the signal photon can interference with itself inside the plate, just like an FP-etalon. Moreover, we observe that the visibility does not change for this kind of modulation. We attribute this situation to the fact that as the free spectral range of the plate ($c/2nl$) is larger than the signal photon bandwidth, only one mode is excited in the plate, and the spectral property of the photon cannot be affected by the plate.

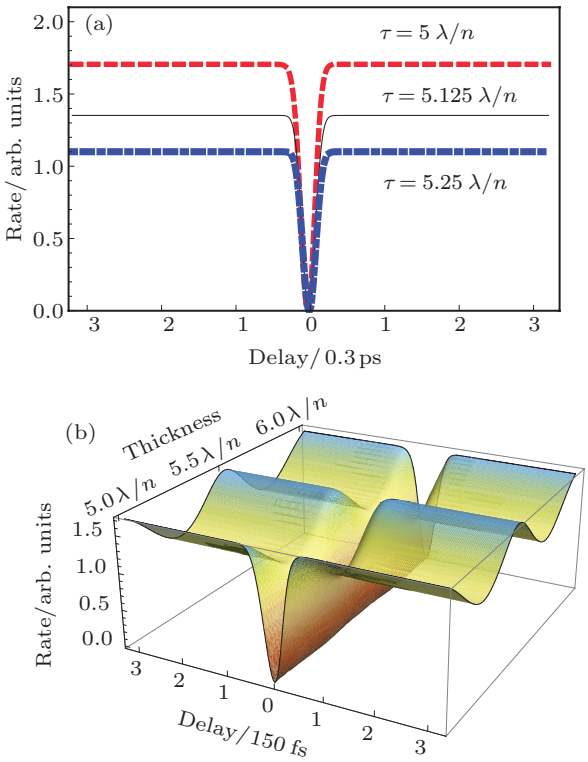


Fig. 2. (colour online) (a) Non-normalized coincidence count rate as a function of delay ($\delta\tau$). The round-trip phase change ($\delta\varphi$) of the signal photon is $2m\pi$, $2m\pi+\pi/2$, and $2m\pi+\pi$ (m is an integer). (b) 3D plot of coincidence count rate as functions of l and $\delta\tau$. $\lambda = 850$ nm, $\Delta\lambda = 10$ nm, $n = 2.1$.

Next, we consider the case of $L = \lambda^2/\Delta\lambda < l$ (denoted by II). In this case, the photons leave the plate separately, and one photon cannot interference with its leading edge. Figure 3 shows a direct numerical calculation derived from Eq. (14). Here $\Delta\lambda$ and n are the same as those in Fig. 2. Figure 3(a) corresponds to the resonance case, i.e., $l = 111.310$ μm and $\delta\phi = 2m\pi$. Figure 3(b) corresponds to the anti-resonance case, i.e., $l = 111.411$ μm and $\delta\phi = 2m\pi+\pi$. We can see that, in Fig. 3(a), there are a series of dips separated by a constant distance; in Fig. 3(b), one dip follows a peak; a dip always occurs first in both cases. The distance between successive dips or a dip and a peak is $\tau_1 = nl/c$, and relative intensity of the dip and peak amplitude are given by Eqs. (B5) and (B6) in Appendix B.

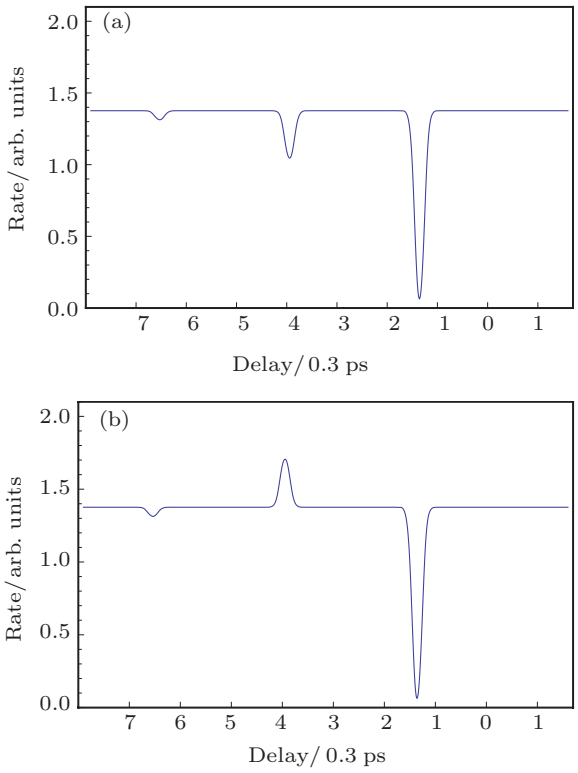


Fig. 3. (colour online) Coincidence count rate as a function of idler delay $\delta\tau$ for $\lambda = 850$ nm. (a) $l = 111.31$ μm, $\delta\phi = 2m\pi$; (b) $l = 111.411$ μm, $\delta\phi = 2m\pi + \pi$.

The interference profiles shown in Fig. 3 are due to the interference mentioned in Ref. [19]. The Feynman space–time diagrams (see Fig. 4) can be used to explain these interference profiles. When the idler delay line is set to satisfy $\delta\tau = \tau_1$, two detection configurations are possible. Both of them consist of two indistinguishable realizations depicted in Figs. 4(a) and 4(b). In Fig. 4(a), detector D1 detects a photon ahead of D2 by a time of τ_1. This can be realized either if the signal photon passes through the plate without reflection, and both photons are reflected by the BS, or in presence of one signal roundtrip inside the plate, and two transmissions through the BS. In Fig. 4(b), detector D2 detects a photon ahead of D1 by the same amount of time. This can be realized either by a single signal roundtrip through the plate and two reflections

on BS, or by transmission through the plate and transmissions of both photons through BS. Whether it is a dip or peak depends on the roundtrip phase change inside the plate, and the k-th dip (or peak) is composed of k diagrams of this type, and the probability amplitude is the sum of all possible paths.

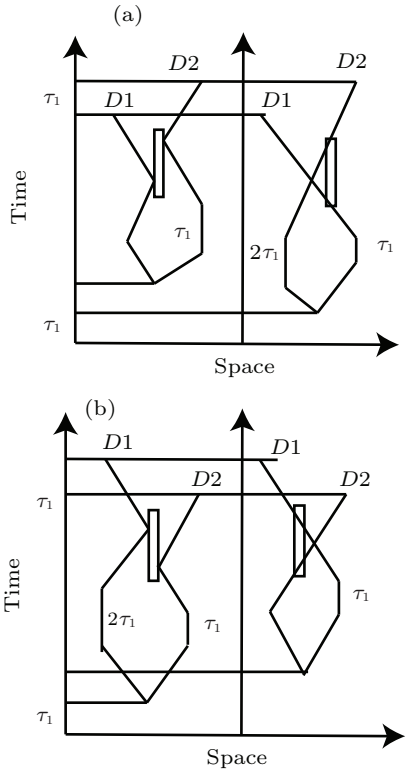


Fig. 4. Feynman-like diagram when the idler delay sets at half a round-trip (τ_1) inside the plate. Each of them is composed of two indistinguishable realizations. (a) Detector D1 detects a photon ahead of D2 by a time of τ_1, (b) detector D2 detects a photon ahead of D1 by τ_1.

Finally, the case (denoted by III) where l is roughly equal to the coherence length is also considered (see Fig. 5). In Fig. 5, $\Delta\lambda$ and n are the same as those in Fig. 2. Figure 5(a) corresponds to the resonance case; figure 5(b) corresponds to the anti-resonance case. We can see that the interference patterns are asymmetry, and oscillation irregularly appears at one side of the dip. This kind of phenomenon may arise from partial interference of the signal photon inside the plate.

5. Coincidence count rate versus plate refractive index

In this section, we study the relation of the coincidence count rate and the plate refractive index n.

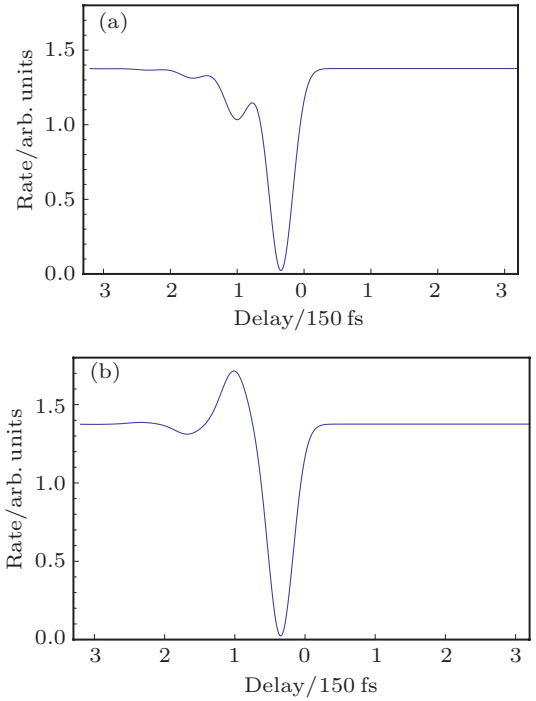


Fig. 5. (colour online) Coincidence count rate as a function of idler delay $\delta\tau$ for $\lambda = 850$ nm. (a) $l = 14.1677$ μm and $\delta\phi = 2m\pi$; (b) $l = 14.2679$ μm and $\delta\phi = 2m\pi + \pi$.

Figure 6 shows the results for $n = 5.5$ and $n = 1.5$ in cases I and II, and the bandwidth is $\Delta\lambda$ =10 nm. Figures 6(a) and 6(b) correspond to the case I, from which we can see that the modulation amplitude in Fig. 6(a) is larger than that in Fig. 6(b), the modulation amplitude $|G(\omega_0)|^2$ in Eq. (16) depends on the value of n, and the ratio of the maximum and minimum value of $|G(\omega_0)|^2$ increases with n. Figures 6(c)–6(f) correspond to the case II. More dips and peaks appear in Figs. 6(c) and 6(d) than in Figs. 6(e) and 6(f). The numbers of dips and peaks that can be seen depend on the relative intensity (see Eqs. (B5) and (B6) in Appendix B) between them. For large n, the reflectivity of the plate is very high, and the amplitude decay between successive wave packets is small. Therefore, we could see more dips (or peaks) in the interference profiles.

6. Coincidence count rate versus IF bandwidth

Now we investigate the influence of the bandwidth of the IF on the coincidence count rate (see Fig. 7). Here we change the bandwidth of the IF, and keep l and n constant ($l = 36.9565$ μm and $n = 2.1$). Only the resonance case is considered. We find from Fig. 7

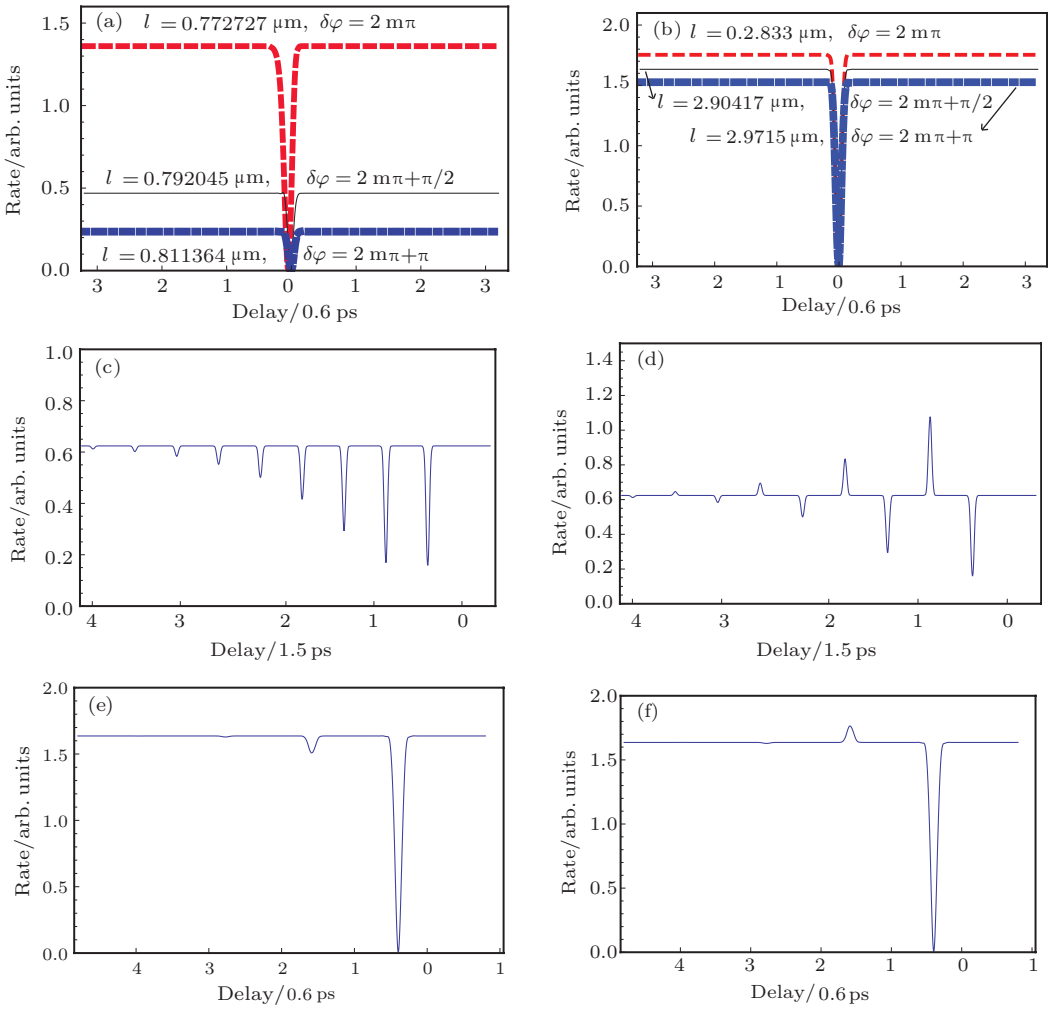


Fig. 6. (colour online) Coincidence count rate as a function of idler delay $\delta\tau$ for $\lambda = 850$ nm and $\Delta\lambda = 10$ nm. (a), (c), and (d) $n = 5.5$; (b), (e), and (f) $n = 1.5$.

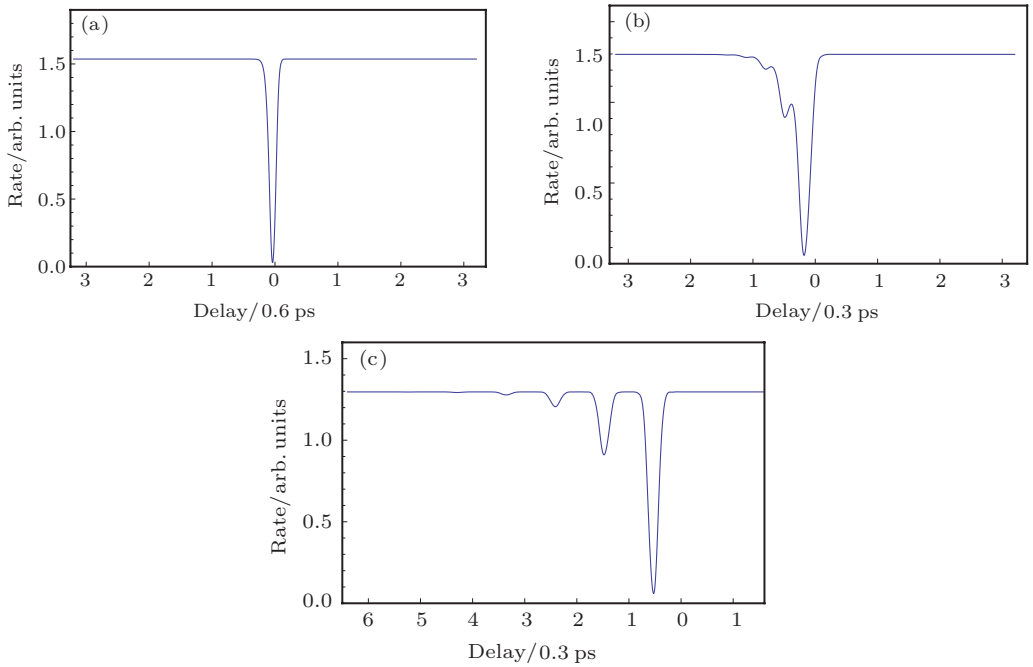


Fig. 7. (colour online) Coincidence count rate as a function of idler delay $\delta\tau$ for $\lambda = 850$ nm and $n = 2.1$. (a) $\Delta\lambda = 1$ nm; (b) $\Delta\lambda = 3$ nm; (c) $\Delta\lambda = 10$ nm.

that the same plate has different responses to the signal photon. Figures 7(a), 7(b), and 7(c) correspond to the cases I, III, and II, respectively. This is not surprising because the bandwidth of the photons in a pair is determined by the bandwidth of the IF. In Fig. 7(a), $\lambda^2/\Delta\lambda \ll l$ is related with the case I; in Fig. 7(c), $\lambda^2/\Delta\lambda \gg l$ corresponds to the case II; In Fig. 7(b), l is about $\lambda^2/\Delta\lambda$, which corresponds to the case III.

7. Conclusion

The quantum response of a dielectric plate has been studied theoretically using a modified HOM interferometer. The fourth-order correlation function is calculated for our model. We find that the plate responses to the same field differently in two cases divided according to the relative size between the thickness of the plate and the one photon-coherent length. When the thickness of the plate is less than the one-photon coherence length, a novel modulation behavior is observed, the modulation amplitude is sensitive to the refractive index of the dielectric plate. The calculated results show that the modulation only changes the intensity of coincidence count rate, but the visibility is independent of this modulation. However, when the thickness of the plate is large than the one-photon coherence length, we observe recurrent dips and peaks due to destructive and constructive interference of different Feynman paths. Moreover, the influences of the refractive of the plate and the bandwidth on the coincidence count rate are discussed. The model we used here may provide potential for application in quantum metrology[20] to characterize the properties of a material. Our results offer an intuitive understanding of the properties of linear optical elements in fourth-order interference.

Appendix A

Derivation of Eq. (12) is given below. Using definition of Eq. (11) and the down-converted two-photon state of Eq. (1), we can calculate $\hat{E}_2^{(+)}(t+\tau)\hat{E}_1^{(+)}(t)\,|\Psi\rangle$ firstly with the help of Eqs. (9) and (10) as

$$\begin{aligned}
&\hat{E}_2^{(+)}(t+\tau)\hat{E}_1^{(+)}(t)\,|\Psi\rangle \\
&= \frac{1}{2}\int \mathrm{d}\omega'(\hat{a}_\mathrm{i}(\omega')\,\mathrm{e}^{-\mathrm{i}\omega'(t+\tau-\tau_1)} \\
&\quad + \mathrm{i}G(\omega')\hat{a}_\mathrm{s}(\omega')\,\mathrm{e}^{-\mathrm{i}\omega'(t+\tau-\tau_1-\delta\tau)})f(\omega') \\
&\quad \times \int \mathrm{d}\omega''(G(\omega'')\hat{a}_\mathrm{s}(\omega'')\,\mathrm{e}^{-\mathrm{i}\omega''(t-\tau_1)} \\
&\quad + \mathrm{i}\hat{a}_\mathrm{i}(\omega'')\,\mathrm{e}^{-\mathrm{i}\omega''(t-\tau_1-\delta\tau)})f(\omega'') \\
&\quad \times \int \mathrm{d}\omega\phi(\omega)\hat{a}_\mathrm{s}^+(\omega)\hat{a}_\mathrm{i}^+(\omega_\mathrm{p}-\omega)\,|\mathrm{vacuum}\rangle. \qquad \text{(A1)}
\end{aligned}$$

The unpaired terms like $\hat{a}_\mathrm{i}\hat{a}_\mathrm{s}$ and $\hat{a}_\mathrm{i}^+\hat{a}_\mathrm{s}^+$ are zero, and the other nonzero terms are

$$\begin{aligned}
&\frac{1}{2}\int_0^{\omega_\mathrm{p}} \mathrm{d}\omega\phi(\omega)G(\omega)f(\omega)f(2\omega_0-\omega) \\
&\quad \times \mathrm{e}^{-\mathrm{i}2\omega_0(t-\tau_1+\tau)+\mathrm{i}\omega\tau}\,|\mathrm{vacuum}\rangle\,, \qquad \text{(A2)} \\
&\frac{1}{2}\int_0^{\omega_\mathrm{p}} \mathrm{d}\omega\phi(\omega)G(\omega)f(\omega)f(2\omega_0-\omega) \\
&\quad \times \mathrm{e}^{-\mathrm{i}2\omega_0(t-\tau_1+\delta\tau)-\mathrm{i}\omega(\tau-2\delta\tau)}\,|\mathrm{vacuum}\rangle\,. \qquad \text{(A3)}
\end{aligned}$$

Substituting $\omega = \omega' + \omega_0$ and $\omega = \omega_0 - \omega'$ to the integral variables of Eqs. (A2) and (A3), respectively, we obtain

$$\begin{aligned}
&\frac{1}{2}\int_{-\omega_0}^{\omega_0} \mathrm{d}\omega'\phi(\omega'+\omega_0)G(\omega'+\omega_0)f(\omega'+\omega_0) \\
&\quad \times f(\omega_0-\omega')\,\mathrm{e}^{-\mathrm{i}2\omega_0(t-\tau_1)+\mathrm{i}\omega'\tau-\mathrm{i}\omega_0\tau}\,|\mathrm{vacuum}\rangle \\
&= \frac{1}{2}\,\mathrm{e}^{-2\mathrm{i}\omega_0(t-\tau_1)-\mathrm{i}\omega_0\tau}\int_{-\omega_0}^{\omega_o} \mathrm{d}\omega\phi(\omega_0+\omega)G(\omega+\omega_0) \\
&\quad \times f(\omega)f(-\omega)\,\mathrm{e}^{\mathrm{i}\omega\tau}\,|\mathrm{vacuum}\rangle \\
&= \frac{1}{2}\,\mathrm{e}^{-2\mathrm{i}\omega_0(t-\tau_1)-\mathrm{i}\omega_0\tau}g_{12}^{(1)}(-\tau)\,|\mathrm{vacuum}\rangle\,, \qquad \text{(A4)} \\
&\quad -\frac{1}{2}\int_{-\omega_0}^{\omega_0} \mathrm{d}\omega'\phi(\omega_0-\omega')T(\omega_0-\omega')f(\omega_0-\omega') \\
&\quad \times f(\omega_0+\omega')\,\mathrm{e}^{-\mathrm{i}2\omega_0(t-\tau_1+\delta\tau)-\mathrm{i}(\omega_0-\omega')(\tau-2\delta\tau)} \\
&\quad \times |\mathrm{vacuum}\rangle \\
&= -\frac{1}{2}\,\mathrm{e}^{-2\mathrm{i}\omega_0(t-\tau_1)-\mathrm{i}\omega_0\tau}\int_{-\omega_0}^{\omega_0} \mathrm{d}\omega\phi(\omega_0-\omega) \\
&\quad \times G(\omega_0-\omega)f(\omega)f(-\omega)\,\mathrm{e}^{\mathrm{i}\omega(\tau-2\delta\tau)}\,|\mathrm{vacuum}\rangle \\
&= -\frac{1}{2}\,\mathrm{e}^{-2\mathrm{i}\omega_0(t-\tau_1)-\mathrm{i}\omega_0\tau}g_{12}^{(2)}(2\delta\tau-\tau)\,|\mathrm{vacuum}\rangle\,. \qquad \text{(A5)}
\end{aligned}$$

The integral range can be expanded from $-\infty$ to $+\infty$. Therefore, the joint probability $P_{12}(\tau)$ is the square of the norm of this state

$$\begin{aligned}
P_{12}(\tau) &\propto \left|\frac{1}{2}\,\mathrm{e}^{-2\mathrm{i}\omega_0(t-\tau_1)-\mathrm{i}\omega_0\tau}[g_{12}^{(1)}(-\tau)\right. \\
&\quad \left. - g_{12}^{(2)}(2\delta\tau-\tau)]\,|\mathrm{vacuum}\rangle\right|^2 \\
&= \frac{1}{4}\left|g_{12}^{(1)}(-\tau)\right|^2 + \frac{1}{4}\left|g_{12}^{(2)}(2\delta\tau-\tau)\right|^2 \\
&\quad - \frac{1}{4}[g_{12}^{(1)}(-\tau)g_{12}^{*(2)}(2\delta\tau-\tau)+\mathrm{c.c.}]. \qquad \text{(A6)}
\end{aligned}$$

Appendix B

We express $G(\omega)$ as

$$G(\omega) = t\exp[\mathrm{i}\omega\tau_0]\sum_{p=0}^{\infty} r^p \exp[2\mathrm{i}p\omega\tau_1], \tag{B1}$$

where $t = 4n/(1+n)^2$, $r = (1-n)^2/(1+n)^2$, $\tau_0 = (n-1)l/c$, and $\tau_1 = nl/c$. Then equation (17) becomes

$$\begin{aligned} R &= t^2 \sum_{p,q} r^{p+q} \exp[2\mathrm{i}(p-q)\omega_0\tau_1] \int \mathrm{d}\omega \\ &\quad \times \exp\left[-\left(\frac{\omega}{\Delta\omega}\right)^2\right](\exp[2\mathrm{i}(p-q)\omega\tau_1] \\ &\quad - \exp\{2\mathrm{i}\omega[\delta\tau + \tau_0 + (p+q)\tau_1]\}) \\ &= C_0 t^2 \sum_{p,q} r^{p+q} \cos[2(p-q)\omega_0\tau_1] \\ &\quad \times (\exp\{-(p-q)^2\Delta\omega^2\tau_1^2\} \\ &\quad - \exp\{-\Delta\omega^2[\delta\tau + \tau_0 + (p+q)\tau_1]^2\}), \end{aligned} \tag{B2}$$

where C_0 is a constant and is neglected. When $\Delta\omega\tau_1 = \Delta\omega nl/c \gg 1$, i.e., in case II, the first term in Eq. (B2) is nonzero only for $p = q$, then Eq. (B2) becomes

$$\begin{aligned} R &= \frac{t^2}{1-r^2} - t^2 \sum_{p,q} r^{p+q} \cos[2(p-q)\omega_0\tau_1] \\ &\quad \times \exp\{-\Delta\omega^2[\delta\tau + \tau_0 + (p+q)\tau_1]^2\}. \end{aligned} \tag{B3}$$

The distance between successive Gaussian functions is τ_1, which is much greater than $1/\Delta\omega$. Hence the overlap between them is small, and can be distinguished. The dip or peak occurs at position $\delta\tau = -\tau_0 - (p+q)\tau_1$, and the maximum amplitude is given by

$$\begin{aligned} R(k) &= \frac{t^2}{1-r^2} - t^2 \sum_{p,q;p+q=k-1} r^{p+q} \\ &\quad \times \cos[2(p-q)\omega_0\tau_1], \end{aligned} \tag{B4}$$

where k is the order of the dip or peak (if $k = 1$, $\delta\tau = -\tau_0$; if $k = 2$, $\delta\tau = -\tau_0 - \tau_1$). The summation is over p and q satisfying $p+q = k-1$. In the resonance case, the cosine function always equals one, and the dip amplitude is

$$R(k) = \frac{t^2}{1-r^2} - t^2 r^{k-1} k. \tag{B5}$$

For anti-resonance case, the amplitude of the dip or peak is given by

$$R(k) = \frac{t^2}{1-r^2} - t^2 (-r)^{k-1} k. \tag{B6}$$

References

[1] Mandel L and Wolf E 1995 *Optical Coherence and Quantum Optics* (Cambridge: Cambridge University Press)

[2] Dauler E, Jaeger G, Muller A and Migdall A 1999 *J. Res. Natl. Stand. Technol.* **104** 1

[3] Migdall A 1999 *Phys. Today* **1** 41

[4] Peřina J, Hradil Z and Jurčo B 1994 *Quantum Optics and Fundamentals of Physics* (Dordrecht: Kluwer)

[5] Bruß D and Lütkenhaus N 2000 *Applicable Algebra in Engineering, Communication and Computing* (vol. 10) (Berlin: Springer) p. 383

[6] Bouwmeester D, Pan J W, Mattle K, Eibl M, Weinfurter H and Zeilinger A 1997 *Nature* **390** 575

[7] Song L J, Yan D and Liu Y 2011 *Acta Phys. Sin.* **60** 120302 (in Chinese)

[8] Giuseppe G D, Haiberger L and Martini F D 1997 *Phys. Rev.* A **56** R21

[9] Olindo C, Sagioro M A, Moken C H and Padua S 2006 *Phys. Rev.* A **73** 043806

[10] Zavatta A, Viciani S and Bellini M 2004 *Phys. Rev.* A **70** 023806

[11] Steinberg A M, Kwiat P G and Chiao R Y 1992 *Phys. Rev.* A **45** 6659

[12] Lu D M 2011 *Acta Phys. Sin.* **60** 090302 (in Chinese)

[13] Lu D M 2011 *Acta Phys. Sin.* **60** 120303 (in Chinese)

[14] Ma S S, Chen M F and Jiang X P 2011 *Chin. Phys.* B **20** 120308

[15] Grunner T and Welsch D G 1996 *Phys. Rev.* A **54** 1661

[16] Kong L Q, Fan L L, Wang A B and Wang Y C 2009 *Acta Phys. Sin.* **58** 7680 (in Chinese)

[17] Hong C K, Ou Z Y and Mandel L 1987 *Phys. Rev. Lett.* **59** 2044

[18] Glauber R J 1963 *Phys. Rev.* **130** 2529

[19] Strekalov D V, Pittman T B and Shih Y H 1998 *Phys. Rev.* A **57** 567

[20] Wiseman H M and Milburn G J 2010 *Quantum Measurement and Control* (Cambridge: Cambridge University Press)